Plane partition vesicles

2006 J. Phys. A: Math. Gen. 39 11171

(http://iopscience.iop.org/0305-4470/39/36/004)

INSTITUTE OF PHYSICS PUBLISHING JOURNAL OF PHYSICS A: MATHEMATICAL AND GENERAL

J. Phys. A: Math. Gen. **39** (2006) 11171–11192 doi:10.1088/0305-4470/39/36/004

Plane partition vesicles

E J Janse van Rensburg and J Ma

Department of Mathematics and Statistics, York University, Toronto, Ontario, M3J 1P3, Canada

E-mail: rensburg@yorku.ca

Received 23 January 2006, in final form 14 July 2006
Published 18 August 2006
Online at stacks.iop.org/JPhysA/39/11171

Abstract

We examine partitions and their natural three-dimensional generalizations, plane partitions, as models of vesicles undergoing an inflation–deflation transition. The phase diagrams of these models include a critical point corresponding to an inflation–deflation transition, and exhibits multicritical scaling in the vicinity of a multicritical point located elsewhere on the critical curve. We determine the locations of the multicritical points by analysing the generating functions using analytic and numerical means. In addition, we determine the numerical values of the multicritical scaling exponents associated with the multicritical scaling regimes in these models.

PACS numbers: 05.50.+q, 02.10.Ab, 05.40.Fb, 82.35.−x

1. Introduction

Random surfaces have received considerable attention in the physics literature as models of fluctuating membranes [1, 12–15]. Closed lattice surfaces in three dimensions are models of lattice vesicles [30] undergoing an inflation–deflation transition. Simple convex versions of these models have also been considered, see for example [18] where cubical and rectangular box lattice vesicles are examined.

In this paper we examine partitions and plane partitions [8] as convex lattice surface models of two-dimensional and three-dimensional vesicles. The model of plane partition vesicles is a generalization of the three-dimensional models in [18]. Plane partitions may be described as the three-dimensional counterparts of partitions, and they can be described as objects composed of unit cubes stacked into a rectangular corner (see figure 1). Two-dimensional lattice polygon models of vesicles, including partitions, were introduced by Brak *et al* who also examined the tricritical nature of critical points in these models; see [5–7].

A model of plane partitions is a convex version of more traditional three-dimensional random surface models of lattice vesicles [2, 29, 30]. Unlike the cubical and rectangular box vesicles studied in [18], there are important conformational entropic contributions to the free energy in models of plane partition vesicles. These contributions will have an effect on the

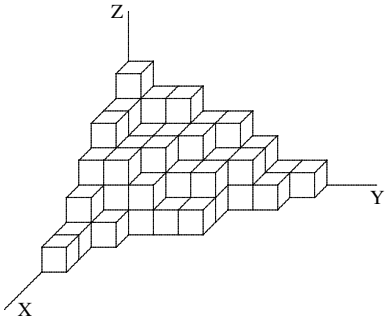

Figure 1. A plane partition. The volume of this plane partition is the total number of unit cubes it contains. Two unit cubes are adjacent if they share a face. A face is paired if it is incident on two cubes, otherwise it is unpaired. The total area of a plane partition is the number of unpaired faces. An edge in a plane partition is regular if it is incident on two unpaired faces, and if these faces are mutually perpendicular. Otherwise it is irregular. The perimeter of a plane partition is the total number of regular edges it contains.

phase behaviour in the model, and will give more insight in the role of conformational degrees of freedom in the thermodynamic behaviour of vesicles undergoing an inflation–deflation transition. Two dimensional partition polygons and three-dimensional plane partition vesicles are also simple enough to be studied extensively by numerical and other means, and to serve as a test bed for the ideas underlying critical scaling in two- and in three-dimensional models of vesicles.

The phase diagram of partition polygons (see figure 5), suggests that the phase diagram of plane partitions may be unusual (see figure 6). Partition polygons in an area–perimeter ensemble undergo an inflation–deflation transition, but the location of this transition is not coincident with a region of multicritical scaling which is located near a singular point elsewhere on the critical curve [6, 7, 16] (see section 2.3 and figure 5). Similar observations have been made in other unrelated lattice models. In particular, the phase diagram of H-bonding self-avoiding walks shows a similar splitting of the critical and a tricritical point [9, 10, 35]. In this paper we examine plane partitions and find a similar splitting of the critical point and a region of multicritical scaling in the vicinity of a singular point elsewhere on the critical curve (see section 4.1 and figure 6).

If a plane partition is composed of n unit cubes, then we say that it is a plane partition of n, or that it has *volume* n (see figure 1). Plane partitions of n were studied by MacMahon in 1887 [25, 27] who discovered the generating function

$$P_p(q) = \sum_{n=0}^{\infty} pp(n)p^n = \prod_{j=1}^{\infty} \frac{1}{(1-p^j)^j} \tag{1}$$

where $pp(n)$ is the number of plane partitions of n (or with volume n), and where we call the generating variable p a 'volume generating variable'. We define $pp(0) = 1$ to be consistent with product generating function above.

Plane partitions played a key role in the alternating sign matrix conjecture [23, 38] and have been the subject of intensive research in the mathematics literature, for a history, see for example [8]. In the physics literature one may find connections to models in statistical mechanics, such as square ice and the six vertex model [23, 39].

Asymptotics for $pp(n)$ can be determined from equation (1). This was for example done by Wright in 1931 [36], and the result is the asymptotic formula

$$pp(n) \approx \frac{K\, \mathrm{e}^{Cn^{2/3}}}{n^{25/36}} \tag{2}$$

obtained by a saddle-point method using a Mellin transform, where $K = 0.400\,99\ldots$ and $C = 2.009\,45\ldots$.

The *surface area* of a plane partition can be defined as follows. Each unit cube in a plane partition has six *faces* (unit squares) and twelve *edges* (unit length line segments) incident on two faces each. A face is *paired* if it is incident on two unit cubes in the plane partition; otherwise it is *unpaired*. The surface area of a plane partition is the total number of unpaired faces. One may similarly define a *perimeter* for plane partitions. An edge in a unit cube in a plane partition is *regular* if it is incident on two unpaired faces, and if these faces are mutually perpendicular. Otherwise it is not regular. The number of regular edges in a plane partition is its perimeter, and it may be interpreted as a measure of the total absolute curvature of the plane partition.

Define $pp(n, m, k)$ to be the number of plane partitions of volume n, area m and perimeter k. For example, $pp(1, 6, 12) = 1$ and $pp(2, 10, 16) = 3$. Define $pp(0, 0, 0) = 1$ trivially to be consistent with the generating function in equation (1). The generating function of plane partitions in the volume–area–perimeter ensemble is

$$P_p(p, q, t) = \sum_{n,m,k \geqslant 0} pp(n, m, k)\, p^n q^m t^k. \tag{3}$$

$P_p(p, q, t)$ is not known in closed form. However, in some cases the generating functions of symmetric and boxed plane partitions have been determined [8]. The generating variables (p, q, t) are conjugate to volume, area and perimeter, respectively.

In this paper we examine scaling of the plane partition generating function in the volume–area ensemble (that is, the generating function $P_p(p, q, 1) \equiv P_p(p, q)$ where we put $t = 1$ in equation (3)). We develop a Metropolis style Monte Carlo algorithm to sample plane partition vesicles along a Markov chain in the volume–area ensemble, and we collect data to examine the properties of $P_p(p, q)$.

In section 2 we review the scaling properties of (two-dimensional) partition polygons. These polygons are convex versions of more general polygons in the square lattice, and such models have been studied since the 1800s [4, 17, 19–22, 26, 31, 33, 34, 37]. The phase diagrams of the generating functions of partition polygons[1] and other convex lattice polygon models in the area–perimeter ensemble are known to include multicritical points [5–7], and in this section we analyse the scaling of the generating functions of partition polygons in the area–perimeter ensemble, $P(q, t)$, in the context of multicritical scaling assumptions [24].

The phase diagram of partition polygons in an area–perimeter ensemble, illustrated in figure 5 and discussed in section 2.3, includes a critical curve on which is located a critical point (t_c, q_c) corresponding to a first order phase transition between deflated and inflated partition polygons. The critical curve is composed of essential singularities in the generating function along the line $q = 1$, which ends in the critical point $(t_c, q_c) = (1, 1)$, where the singularities change over into simple poles along the curve $t^2 q = 1$. This point is a tricritical point, which is defined as the endpoint of a line of first order transitions from which starts a line of continuous transitions; see [24], and in particular figure 10 in that reference. The

[1] The generating function of partition polygons is $P(q, t)$, where q is an area generating variable, and t is a perimeter generating variable. We shall consistently indicate generating functions of plane partition vesicles by a subscript 'p'. For example, $P_p(q, t)$ is the generating function of plane partition vesicles in the area–perimeter ensemble, while $P_p(p, q)$ is the generating function of plane partition vesicles in the volume–area ensemble.

phase diagram in figure 5 is unusual [16] in that there is a second point on the critical curve, not coincident with the tricritical point $(1, 1)$, about which the generating function exhibits multicritical scaling. We review the scaling around this point and show why the crossover exponent in this model is generally accepted to be $\phi = 1/2$.

In section 3 we introduce a model of plane partition vesicles and a Metropolis Monte Carlo algorithm for sampling along a Markov chain in the state space of plane partition vesicles weighted by volume, area and perimeter. In section 4 we examine the scaling of plane partition vesicles numerically in the volume–area ensemble. The phase diagram is illustrated in figure 6, and we discuss it in section 4.1. The critical curve in this model is composed of essential singularities along $p = 1$ for $0 \leqslant q \leqslant 1$, and these changes into simple poles along the curve $q^4 p = 1$ if $q > 1$ in the critical point $(q_c, p_c) = (1, 1)$. This is a tricritical point, where a line of first order transitions ends and from which curves of continuous transitions starts in higher dimensional parameter space [24].

We examine the scaling of the plane partition generating function $P_p(1, q)$ along the line $p = 1$ next. Scaling assumptions along this line is analogous to the scaling of partition polygons, and our data show that $P_p(1, q)$ diverges as $q \nearrow q_t$ where

$$q_t = 0.846\,70 \pm 0.000\,28, \tag{4}$$

and we note that $q_t \approx \sqrt{3}/2$. This behaviour is consistent with the results for partition polygons, and is also consistent with multicritical scaling in the vicinity of the point $(q_t, p_t) = (q_t, 1)$.

Our simulations provide strong evidence that the mean area of plane partition vesicles along the line $p = 1$ diverges as

$$\langle \text{Area} \rangle \sim [-\log(q/q_t)]^{-\rho} \qquad \text{as} \quad q \nearrow q_t, \tag{5}$$

where $\rho = 1.3449 \pm 0.0020 \approx 4/3$. This inverse power-law divergence in the mean area has certain implications for scaling of the generating function, and we use this result to estimate the value of multicritical scaling exponents in this model.

Next, plane partition vesicles were examined along the line $q = q_t$ and $0 < p < 1$. We provide numerical evidence showing that the mean volume of plane partitions diverges as

$$\langle \text{Volume} \rangle \sim [-\log p]^{-2} \qquad \text{as} \quad p \nearrow 1. \tag{6}$$

From these results one may estimate the values of the multicritical exponents numerically. In particular, we argue that our results are consistent with the scaling

$$P_p(1, q) \sim \mathrm{e}^{\alpha/[-\log(q/q_t)]^{1/3}} / [-\log(q/q_t)]^{2.0} \tag{7}$$

$$P_p(p, q_t) \sim \mathrm{e}^{\beta/[-\log p]} / [-\log p]^{0.88}, \tag{8}$$

of the generating function, where $q_t \approx \sqrt{3}/2$. Overall, our results suggest that there is a multicritical point located at $(p_t, q_t) = (1, \sqrt{3}/2)$ with a crossover exponent ϕ approximately equal to $1/2$, in addition to the tricritical point at the endpoint of the line of essential singularities along $p = 1$ in figure 6.

A few conclusions are given in section 5. We examine plane partitions briefly from a perimeter activity point of view. Our algorithm did not converge well in this ensemble, and the quality of numerical data was not good enough to extract estimates of exponents. However, our results do show that the generating function $P_p(1, 1, t)$ becomes singular as t approaches the point $t = 3^{-1/4}$, and we conjecture that the critical value of the perimeter fugacity t is given by $t_t = 3^{-1/4}$. This result, together with $q_t = \sqrt{3}/2$, gives the locations of multicritical points and scaling regimes in the pq-, pt- and qt-ensembles.

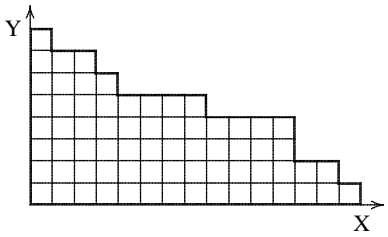

Figure 2. A partition polygon. Each unit square in this polygon is weighted by the area generating variable q, and each perimeter edge is weighted by t, the perimeter generating variable.

2. Partition polygons

2.1. The generating function of partition polygons

The two-dimensional version of a plane partition vesicle in a volume–area–perimeter ensemble is a partition polygon in an area–perimeter ensemble. An example of a partition polygon is given in figure 2. The area of the polygon is the number of unit squares that paves its interior. An *unpaired edge* is an edge in the boundary of a unit square that is incident with only one unit square in the interior of the partition polygon. The perimeter of the partition polygon is the union of all unpaired edges, and it is a lattice polygon. The length of the perimeter is the number of edges in the perimeter.

Partition polygons have been studied as two-dimensional models of vesicles in the 1990s [3, 5, 7]. The generating function of this model is given by

$$P(q,t) = \sum_{n=0}^{\infty} \frac{q^{n^2} t^{4n}}{(t^2 q;q)_n^2} \tag{9}$$

where the q-analogue of the factorial is defined by

$$(t;q)_n = \prod_{i=0}^{n-1} (1 - tq^i), \tag{10}$$

and q is the area generating variable, while t is the perimeter generating variable.

If $t = 1$ in equation (9), then the generating function of partitions is obtained [27]. Several expressions are known, and in particular

$$P(q,1) = \sum_{n=0}^{\infty} \frac{q^{n^2}}{(q;q)_n^2} = \prod_{n=0}^{\infty} \frac{1}{(q;q)_n}. \tag{11}$$

The asymptotic behaviour of partitions have been extracted from its generating function when $t = 1$ by Hardy and Ramanujan [11] who derived the asymptotic formula

$$p_n \sim \frac{1}{4\sqrt{3}n} \, \mathrm{e}^{\pi\sqrt{2n/3}} \tag{12}$$

for the number of partitions p_n of n [11].

The function $P(q,1)$ can be approximated by an integral, and a saddle point approximation [7, 16, 32] of this integral shows that as $q \to 1^-$,

$$P(q,1) \sim \frac{\exp(\mathcal{L}i_2(q)/|\log q|)}{\sqrt{|\log q|}}. \tag{13}$$

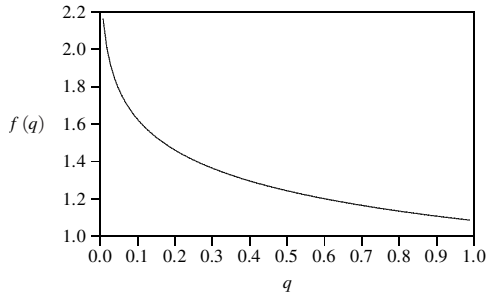

Figure 3. The function $f(q)$, estimated numerically.

The dilogarithm is defined by $\mathcal{L}i_2(q) = \sum_{m=1}^{\infty} q^m/m^2$, see for example [16] (a factor of $\pi^2/6$ was inserted incorrectly in equation (4.23) in that reference). The saddle point approximation only estimates the dominant part of an integral approximation to $P(q, 1)$, but this approximation does capture the general behaviour of the function. To illustrate this, define the function $f(q)$ by

$$P(q, 1) = \frac{\exp(\mathcal{L}i_2(q)/|\log q|)}{f(q)\sqrt{|\log q|}}. \tag{14}$$

Then $f(q)$ should be bounded as $q \to 1^-$. A numerical evaluation of $f(q)$ is plotted in figure 3.

The Euler–Maclaurin formula may instead be used to determine a uniform asymptotic expression for $\log P(q, 1)$. The result is

$$\log P(q, 1) = \frac{\mathcal{L}i_2(q)}{|\log q|} - \frac{\log(1-q)}{2} + R_1 \tag{15}$$

where the remainder is bounded uniformly in $[0, 1]$ by $|R_1| \leqslant 1/12$. This result is consistent with equation (13), and it proves that $f(q)$ is bounded by a constant as $q \nearrow 1$ in equation (14).

One may similarly determine an approximation to $P(q, t)$ by approximating the series by an integral and then by estimating the integral with a saddle-point approximation. This approximation turns out to be in particular valid if $t \in (1/\sqrt{2}, 1)$ and it is given by [16]

$$P(q, t) \approx \sqrt{\frac{2\pi(1-t^2)}{|\log q|(1-t^2q)}}\exp((\mathcal{L}i_2(t^2q) + \mathcal{L}i_2(t^2) + 4(\log t)^2 - \pi^2/6)/|\log q|). \tag{16}$$

This approximation should be good for q and t smaller than 1 but approaching it. For example, $P(0.95, 0.85) = 1552.21\ldots$ while equation (16) gives 1517.67, and $P(0.95, 0.90) = 2.1491\ldots \times 10^5$ while equation (16) gives $2.0760\ldots \times 10^5$.

2.2. The critical curve

The *critical curve* $q_c(t)$ of partition polygons in an area–perimeter ensemble is the radius of convergence of $P(q, t)$, plotted in the tq-plane. It follows directly from equation (9) that

$$q_c(t) = \begin{cases} 1, & \text{if } 0 < t \leqslant 1, \\ \dfrac{1}{t^2}, & \text{if } t > 1. \end{cases} \tag{17}$$

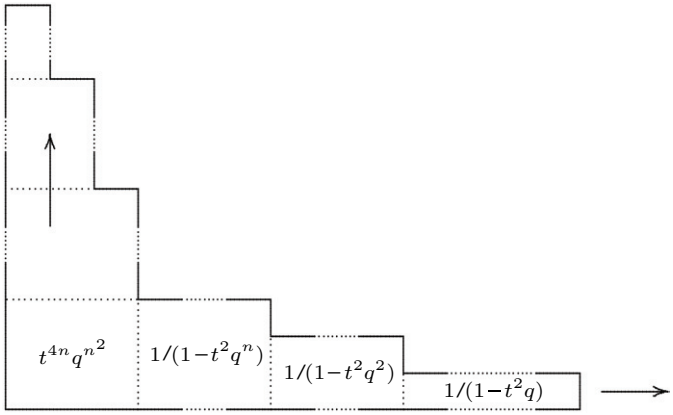

Figure 4. The generating function $P(q,t)$ contains factors $t^{4n}q^{n^2}$ which corresponds to the square in the left lower corner of this illustration of a partition polygon. The factors $1/(1-t^2q^n)$ generate rectangular parts of arbitrary length in the two 'arms' (one horizontal, and the other vertically oriented) of the partition attached to a square of area n^2. By putting $q=1$ and summing over n, the result is equation (18), and the critical point is at $t_t = 1/\sqrt{2}$. Increasing $t \nearrow 1/\sqrt{2}$ with $q=1$ gives divergent factors $1/(1-2t^2)$; these correspond to the uncontrolled lengthening of the 'arms' in this schematic illustration.

If $q=1$, then equation (9) may be evaluated in closed form. The result is

$$P(1,t) = \frac{(1-t^2)^2}{1-2t^2}. \tag{18}$$

This shows that if $t \nearrow 1/\sqrt{2}$ along the line $q=1$, then $P(1,t)$ diverges. This divergence in $P(1,t)$ is due to the unbounded expansion of long and thin rectangular sections of the partition polygon. Thus, along the line $q=1$, $P(q,t)$ is finite for $t \in [0, 1/\sqrt{2})$, and it has a simple pole in the t-plane at $t = 1/\sqrt{2}$. For values of t larger than $1/\sqrt{2}$, $P(q,t)$ is divergent if $q=1$.

Along the curve $q = 1/t^2$ the factor $1/(1-t^2q)$ diverges in equation (9). This factor corresponds to a sequence of unit squares, which diverges as $t^2q \to 1^-$ (see figure 4). Thus $P(q,t)$ is divergent on approach to this curve.

A plot of $q_c(t)$ in the qt-plane is the *phase diagram* of partition polygons. This is given in figure 5. The generating function also has simple poles in the q-plane at the points $t^2q^n = 1$ for $n = 1, 2, 3, \ldots$. In the tq-plane these accumulate on the line $q=1$, so that the unit disc is the natural boundary of the generating function in the q-plane.

The curve $q_c(t)$ divides the tq-plane in figure 5 into two phases. The first is a phase of 'finite' partition polygons for points (t,q) in the area defined by the region enclosed by the axes and the critical curve $q_c(t)$ (see figure 5). The second phase is the region where (t,q) is a point above the critical curve $q_c(t)$ in figure 5. This is a phase of 'infinite' partition polygons.

2.3. The multicritical scaling of $P(q,t)$

The phase diagram is plotted in figure 5. The critical curve $q_c(t)$ is separated into two parts by the critical point at (t_c, q_c). The first part is the line segment along $q=1$ and this is a line of essential singularities in the q-plane corresponding to first order phase transitions (marked

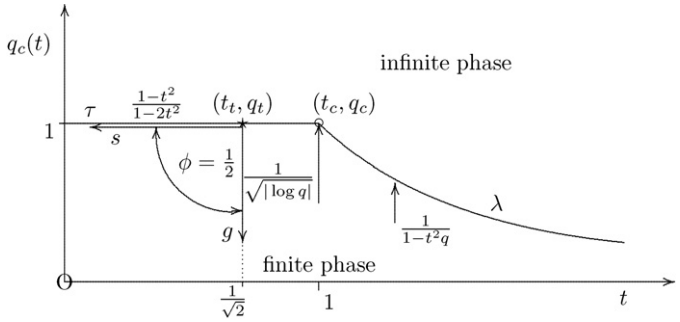

Figure 5. A schematic plot of $q_c(t)$. This is also the phase diagram of partition polygons in an area–perimeter ensemble, with the phase boundary $q_c(t)$ separating a finite and an infinite phase. The critical curve $q_c(t)$ is a line of essential singularities in the generating function from $(0, 1)$ to the critical point at $(1, 1)$ where it ends in a tricritical point $(t_c, q_c) = (1, 1)$ and from where it continues as a curve of simple poles in the generating function along the curve $t^2 q = 1$; see [24]. The generating function is finite on $q_c(t)$ for $t \in [0, t_t)$, but diverges as $e^{C/|\log q|}/\sqrt{|\log q|}$ for $t \in [t_t, 1)$. In this model we set up scaling axes at the multicritical point (t_t, q_t). The g-axis is transverse to the critical curve and points down, while the s-axis is along the line $q = 1$, but pointing towards the left. The generating function $P(q, t)$ diverges along the g- and s-axes on approaching the multicritical point. Standard multicritical scaling ansatz indicates that one may assign the values $2 - \alpha_t = -1/2$ and $2 - \alpha_u = -1$ for the multicritical exponents α_t and α_u. The crossover exponent can be determined from these values: $\phi = 1/2$ in this model. There is a first order phase transition in model at the critical point $(t_c, q_c) = (1, 1)$, where the vesicle undergoes an inflation–deflation transition.

by τ in figure 5) in the model. This line of first order transitions ends in the tricritical point $(t_c, q_c) = (1, 1)$ and continues from there along the curve $qt^2 = 1$ as continuous transitions (marked by λ in figure 5). This should be compared to figure 10 in [24].

The critical curve $q_c(t)$ has two points of potential interest. The first point is the tricritical point at $(t_c, q_c) = (1, 1)$. At this point the nature of the singularity along $q_c(t)$ changes from an essential singularity along the line $q = 1$ to a simple pole along the curve $q = 1/t^2$. Normally, tricritical scaling is expected in the vicinity of such a point [7, 24, 32].

There is a second point of interest. This is the point on the line $q = 1$ at $(t_t, q_t) = (1/\sqrt{2}, 1)$. At this point the function $P(1, t)$ has a pole in the t-plane (see equation (18)) and as we shall see below, the generating function has asymptotic behaviour in the vicinity of this point consistent with multicritical scaling [24], and with identifiable multicritical exponents.

Consider $P(q, t)$ close to the point $(t_t, q_t) = (1/\sqrt{2}, 1)$. Along the line $q = 1$ the generating function $P(1, t)$ diverges as a simple pole as $t \nearrow 1/\sqrt{2}$; see equation (18). Along the line $t = 1/\sqrt{2}$ the behaviour of $P(q, t)$ as $q \to 1^-$ is given by (16) with $t^2 = 1/2$. Simplify matters by ignoring those factors in this expression which approach constants as $q \to 1^-$. Then

$$P(q, 1/\sqrt{2}) \sim \frac{1}{\sqrt{|\log q|}} \exp(C/|\log q|), \qquad \text{as} \quad q \to 1^-. \tag{19}$$

Canonical multicritical scaling assumptions [24] in this model would define two scaling axes (the g-axis and s-axis) through the point $(t_t, q_t) = (1/\sqrt{2}, 1)$. The g-axis is transverse to the critical curve, and the s-axis is tangent to it; as illustrated in figure 10 in [24]. The origin in the gs-plane is located at the point $(t, q) = (1/\sqrt{2}, 1)$. Examination of equations (18)

and (19) suggests the choices $g = |\log q|$ and $s = (1 - 2t^2)$ as scaling variables. Then equations (18) and (19) become

$$P(1,t) \sim \frac{1}{s} \text{ and } P(q, 1/\sqrt{2}) \sim \frac{1}{\sqrt{g}}\, \mathrm{e}^{C/g}, \qquad \text{as} \quad g \to 0^+ \text{ and } s \to 0^+. \tag{20}$$

Multicritical scaling assumptions introduce the exponents $2-\alpha_t$ and $2-\alpha_u$ by assuming that $P(g,s) \equiv P(q,t)$ scales with g and s as power laws given by

$$\begin{aligned} P(q, 1/\sqrt{2}) = P(g,0) &\sim g^{2-\alpha_t}, \qquad \text{as} \quad g \to 0^+, \\ P(1,t) = P(0,s) &\sim s^{2-\alpha_u}, \qquad \text{as} \quad s \to 0^+, \end{aligned} \tag{21}$$

along the g and s axes. These power-law dependences of $P(q,t)$ on g and s close to the point $(g,s) = (0,0)$ should be compared to equation (20) to determine the values of $2-\alpha_t$ and $2-\alpha_u$. The scaling assumptions in equation (21) further imply that $P(q,t)$ is a function of a combined variable $g^{-\phi}s$ such that there exists a scaling function $F(x)$ such that

$$P(q,t) \sim g^{2-\alpha_t} F(g^{-\phi}s). \tag{22}$$

Consistency with equations (21) requires that

$$\phi = \frac{2-\alpha_t}{2-\alpha_u}. \tag{23}$$

The exponent ϕ is the *crossover exponent* describing the crossover of scaling behaviour as the scaling of $P(q,t)$ around the multicritical point is changed from one scaling direction to the other.

The scaling laws in equation (21) appear not to describe the scaling of $P(q,t)$ in equation (20). In particular, there is extra factor of $\mathrm{e}^{C/g}$ which modifies the power-law behaviour (apparently dramatically) as $g \to 0^+$, unless C approaches zero fast enough in this regime. Thus one may propose the alternative scaling relation

$$P(q, 1/\sqrt{2}) = P(g,0) \sim g^{2-\alpha_t}\, \mathrm{e}^{C/g}. \tag{24}$$

The function C may be estimated by examining equation (16). Observe that $\mathcal{L}i_2(1/2) = \pi^2/12 - [\log 2]^2/2$ and assume that $q \approx 1^-$. Then

$$\mathcal{L}i_2(q/2) + \mathcal{L}i_2(1/2) + [\log 2]^2 - \pi^2/6 = |\log q| \log 2 + |\log q|^2 (1 - \log 2)/2 + O(|\log q|^3), \tag{25}$$

so that $C \to 0^+$, as $q \to 1^-$.

In other words $C/g = \log 2 + g(1 - \log 2)/2 + O(g^2)$, and this result shows that the proposed scaling $P(g,0) \sim g^{2-\alpha_t}\, \mathrm{e}^{C/g}$ in equation (24) may be reduced to the standard assumption in equation (21). Some care is necessary though, C/g approaches $\log 2$ linearly with g, and its effects could influence numerical determinations of $P(q,t)$ even close to the multicritical point at $(t_t, q_t) = (1/\sqrt{2}, 1)$.

Thus, one may examine the scaling of partition polygons close to the point at $(t_t, q_t)) = (1/\sqrt{2}, 1)$ by firstly relying on equation (16) to guess that $C/g = \log 2 + g(1 - \log 2)/2 + O(g^2)$, or secondly by assuming that $C/g \approx \log 2$ in equation (24), and then ignoring the contribution of the exponential factor in equation (24). This would suggest that one may choose one of two possible scaling assumptions

$$P(q,t) \sim \begin{cases} [1/\sqrt{g}] \exp((\mathcal{L}i_2(q/2) + \mathcal{L}i_2(1/2) + \log^2 2 - \pi^2/6)/g F(g^{-1/2}s)), \\ [1/\sqrt{g}] F(g^{-1/2}s), \end{cases} \tag{26}$$

Table 1. $F(g^{-1/2}s)$ along the curve $g^{-1/2}s = 1$.

q	t	g	s	$F(1)$ by equation (29)
0.50	0.2893	0.693 1	0.832 6	0.8357
0.60	0.3777	0.510 8	0.714 7	0.7252
0.70	0.4488	0.356 7	0.597 2	0.6206
0.80	0.5136	0.223 1	0.472 4	0.5169
0.90	0.5811	0.105 4	0.324 6	0.4056
0.95	0.6219	0.051 29	0.226 5	0.3393
0.97	0.6424	0.030 46	0.174 5	0.3067
0.99	0.6707	0.010 05	0.100 3	0.2633
0.995	0.6816	0.005 013	0.070 80	0.2472
0.999	0.6958	0.001 001	0.031 63	0.2266
0.9995	0.6992	0.000 5001	0.022 36	0.2218

in the vicinity of the point $(t_t, q_t) = (1/\sqrt{2}, 1)$ where $F(x)$ is some universal function approaching a constant as $x \to 0^+$, and which describes crossover scaling. Comparison with equations (16) and (20) shows that

$$2 - \alpha_t = -1/2, \qquad 2 - \alpha_u = -1, \qquad \phi = 1/2 \tag{27}$$

where the crossover exponent ϕ was determined from equation (23).

Equation (22) indicates that one should be interested in the behaviour of $P(q, t)$ along the curves $g^{-1/2}s = \text{const}$. Then $F(g^{-1/2}s)$ is constant, and the square root scaling in g should be exposed. In table 1 the numerical approximation to $F(g^{-1/2}s)$ is given along the curve $g^{-1/2}s = 1$. One would expect $F(g^{-1/2}s)$ to approach a non-zero constant as $q \to 1^-$ along the curve $g^{-1/2}s = 1$ for both the expressions

$$F(g^{-1/2}s) \sim \sqrt{g}\exp(-(\mathcal{L}i_2(q/2) + \mathcal{L}i_2(1/2) + \log^2 2 - \pi^2/6)/g)P(q, t) \tag{28}$$

and

$$F(g^{-1/2}s) \sim \sqrt{g}P(q, t). \tag{29}$$

Observe that as $q \to 1^-$ and as the multicritical point $(t_t, q_t) = (1/\sqrt{2}, 1)$ is approached, then both the expressions above approach constants, but there are also unaccounted for corrections in this scaling.

Next, consider the tricritical point at $(t_c, q_c) = (1, 1)$. One may set up a g-axis by defining the coordinate $g = |\log q|$. Since $\mathcal{L}i_2(g) = |\log q| + |\log q|^2/4 + O(|\log q|^2)$, the approximation in equation (13) may be written in terms of the scaling field g as

$$P(q, 1) \sim \frac{\exp(1 + |\log q|/4)}{\sqrt{g}} = \frac{\mathrm{e}^{1+g/4}}{\sqrt{g}}. \tag{30}$$

This shows a power-law divergence in $P(q, 1)$ as $q \to 1^-$ similar to equation (20); one may assign the value $2 - \alpha_t = -1/2$ here as well.

It is not possible to define a second scaling axis at this point as we did at the point $(t_t, q_t) = (1/\sqrt{2}, 1)$. $P(q, t)$ is already infinite along $q = 1$ close to $t = 1$, and there is no scaling along this axis. Overall the situation is as illustrated in figure 5. There is multicritical scaling around the point $(t_t, q_t) = (1/\sqrt{2}, 1)$. However, this point does not coincide with the critical point at $(t_c, q_c) = (1, 1)$ at which the system exhibits a phase transition between deflated and inflated phases. The model of partition polygons is atypical in this respect, and it shares this feature with stack polygons [16].

Lastly, the inverse square root scaling in the g-coordinate is apparently preserved along the line $q = 1$ for $t \in [1/\sqrt{2}, 1]$. In this sense one may argue that the multicritical scaling region extends in the vicinity of the line segment $q = 1$ and $t \in [1/\sqrt{2}, 1]$ in this model.

2.4. The limiting free energy of partition polygons

The limiting free energy of partition polygons is defined by first defining the partition function

$$Z_n(t) = \sum_{m=0}^{\infty} p(n, m)t^m \tag{31}$$

where $p(n, m)$ is the number of partition polygons of area n and perimeter m. The limiting free energy is defined from the partition function in the usual way:

$$\mathcal{F}(t) = \lim_{n\to\infty} \frac{1}{n} \log Z_n(t). \tag{32}$$

It follows directly from the definition of $P(q, t)$ that

$$\mathcal{F}(t) = -\log q_c(t) \tag{33}$$

where $q_c(t)$ is the radius of convergence of $P(q, t)$ which we determined above.

In this model,

$$\mathcal{F}(t) = \begin{cases} 0, & \text{if } 0 < t \leqslant 1, \\ 2\log t, & \text{if } t > 1. \end{cases} \tag{34}$$

There is a non-analyticity at $t = 1$ in this function: at this point there is a first order phase transition in the model from inflated partition polygons with large area (dominating the generating function along the line $q = 1$) to deflated polygons with small area along the curve $q = 1/t^2$.

The crossover exponent is related to α, the specific heat exponent, through the hyperscaling relation $2-\alpha = 1/\phi$, and this shows that $\alpha = 0$ in this model. However, it is not clear that this estimate of α, made by examining multicritical scaling in the vicinity of the point (t_t, q_t), is associated with the thermodynamics of the phase transition in partition polygons at the critical point (t_c, q_c).

3. Monte Carlo simulations of plane partitions

We now turn our attention to plane partition models of three-dimensional lattice vesicles. Less is known about these models, and it is not possible to give an explicit analysis of multicritical scaling in this model as we did for partition polygons in section 2. Instead, we approach the model numerically.

A Monte Carlo sampling scheme for plane partition vesicles can be implemented via the Metropolis algorithm to sample plane partitions along a Markov chain. The plane partition vesicles will be weighted by volume, area and perimeter activities (p, q, t).

The state space of the algorithm will be the set of all plane partitions endowed with the distribution

$$D(p, q, t) = \frac{pp(n, m, k)p^n q^m t^k}{P_p(p, q, t) - 1} \tag{35}$$

where $P_p(p, q, t) - 1$ is the normalizing factor given by equation (3), and $pp(n, m, k)$ is the number of plane partitions with volume n, area m and perimeter k. We subtract 1 in the denominator because the algorithm will not be able to generate the empty plane partition.

Algorithm plane partition is implemented as follows:

Algorithm plane partition. Suppose that states $\rho_1, \rho_2, \rho_3, \ldots, \rho_n$ have been sampled along a Markov chain by algorithm plane partition, and that ρ_n is the current state. Suppose that the volume of ρ_n is $V(\rho_n)$, that its area is $A(\rho_n)$, and that its perimeter is $S(\rho_n)$.

Then state ρ_{n+1} is constructed as follows:

1. Select one of the XY-, XZ- or YZ-planes with probability $1/3$, and project ρ_n onto it. The image is a partition P of area (say) α.
2. Choose a unit square σ with uniform probability in P. This square is the projected image of a column γ of unit cubes in ρ_n. Let the height of this column be $h(S)$.
3. With probability $1/2$ attempt to remove the top unit cube in γ; this will reduce $h(S)$ by 1. Alternatively, with probability $1/2$ attempt to add a unit cube onto the top of γ; this will increase $h(S)$ by 1.
4. If the operation in step 3 produces an object which is not a plane partition, or if it changes the projection of ρ_n (this could occur if $\rho(S) = 1$, and a cube is removed), then reject the attempted move. Put $\rho_{n+1} = \rho_n$ to find the next state and go to step 1.
5. Otherwise, a possible next state ρ' is obtained. Accept ρ' as the next state with probability
$$P(\rho_n \to \rho') = \min\left\{1,\, p^{V(\rho')-V(\rho_n)} q^{A(\rho')-A(\rho_n)} t^{S(\rho')-S(\rho_n)}\right\} \tag{36}$$
by generating a random number x and putting $\rho_{n+1} = \rho'$ if $x \leqslant P(\rho_n \to \rho')$, and $\rho_{n+1} = \rho_n$ otherwise.
6. The new current state is then ρ_{n+1}. Continue the sampling by returning to step 1 until a desired number of states are sampled.

Algorithm plane partition is irreducible since any plane partition can be reduced to a single cube by applying the elementary move. The rejection technique ensures that the algorithm is aperiodic, so that the algorithm is ergodic. Next, it may be checked that the algorithm satisfies a condition of detailed balance given by

$$p^{V(\rho_n)} q^{A(\rho_n)} t^{S(\rho_n)} P(\rho_n \to \rho_{n+1}) = p^{V(\rho_{n+1})} q^{A(\rho_{n+1})} t^{S(\rho_{n+1})} P(\rho_{n+1} \to \rho_n). \tag{37}$$

Thus, by the fundamental theorem of Markov chains, the invariant distribution of algorithm plane partition is given by equation (35).

Sampling with the algorithm realizes a stationary Markov chain of states $\{\rho_n\}$. If X is an observable along this chain, then its mean $\langle X\rangle$ is estimated by the unbiased average

$$\langle X\rangle_N = \frac{1}{N}\sum_{i=1}^{N} X(\rho_i). \tag{38}$$

A 67% statistical confidence interval can be estimated from the standard deviation σ of the chain, estimated by

$$\sigma_N^2 = \frac{1}{N-1}\sum_{i=1}^{N}(X(\rho_i) - \langle X\rangle)^2 \tag{39}$$

where $\langle X\rangle$ may be replaced by $\langle X\rangle_N$ for large N as a good approximation. Then $\sigma_N \to \sigma$ as $N \to \infty$, and for large N the 67% confidence interval is approximated well by $\sqrt{2\tau\sigma_N^2}$ where τ is the autocorrelation time measured along the Markov chain. For details, see [28].

The algorithm was tested by generating plane partition vesicles with distribution $D(p, 1, 1)$ (see equation (35)). The mean volume of plane partition vesicles generated by the algorithm at activity p is given by

$$V_p = \frac{\mathrm{d}}{\mathrm{d}\log p}\log(P_p(p, 1, 1) - 1). \tag{40}$$

Table 2. Plane partition volumes by Monte Carlo.

p	Volume by algorithm	V_p by equation (40)
0.60	17.924 ± 0.069	17.87
0.70	52.65 ± 0.26	52.75
0.80	215.80 ± 0.78	216.0
0.85	562.9 ± 6.1	559.6
0.90	2056 ± 11	2055

This may be estimated numerically for given p, and the results may be compared to estimates computed by algorithm plane partition. These quantities are listed in table 2. The error bars in that table are 67% statistical confidence intervals. These data verify the algorithm.

4. Numerical simulations of plane partition vesicles

The determination of the phase diagram and multicritical scaling of plane partition vesicles should ideally be approached as in section 2. Unfortunately, the generating function in the volume–area–perimeter ensemble is only partially known for this model, and is given by equation (1). Analysing $P_p(p)$ would give information about scaling along the p-axis; but it would not be possible to determine scaling and crossover exponents in the model if area and perimeter generating variables are also introduced. Moreover, the location of a multicritical point or region is not known; this considerably complicates matters.

4.1. Plane partition vesicles in the volume-area ensemble

Consider $P_p(p, q, t)$ in equation (3) and consider the case that $t = 1$. Define the generating function $P_p(p, q) \equiv P_p(p, q, 1)$. The maximum area of a plane partition composed of n unit cubes is $4n + 2$ (when the plane partition is a straight row of n cubes). This shows that

$$P_p(p, q) \geqslant \sum_{n>0} p^n q^{4n+2}, \tag{41}$$

and the series $P_p(p, q)$ is divergent if $pq^4 > 1$.

On the other hand, there exists plane partition vesicles of volume n^3 and area $6n^2$ (these are cubical in shape), so that

$$P_p(p, q) > \sum_{n>0} p^{n^3} q^{6n^2}. \tag{42}$$

Thus the generating function is divergent if $p > 1$. Observe also that

$$P_p(p, q) \leqslant \sum_{n\geqslant 0} pp(n) p^n q^{4n+2} \qquad \text{if} \quad q \geqslant 1, \tag{43}$$

where $pp(n)$ is the number of plane partitions of volume n. Since $pp(n) \sim \mathrm{e}^{o(n)}$ by equation (2), it follows that $P_p(p, q) < \infty$ if $pq^4 < 1$ and $q \geqslant 1$. Thus, the radius of convergence of $P_p(p, q)$ is given by

$$p_c(q) = \begin{cases} 1, & \text{if } q \leqslant 1, \\ \dfrac{1}{q^4}, & \text{if } q > 1. \end{cases} \tag{44}$$

This is the critical curve of $P_p(p, q)$ in the pq-plane.

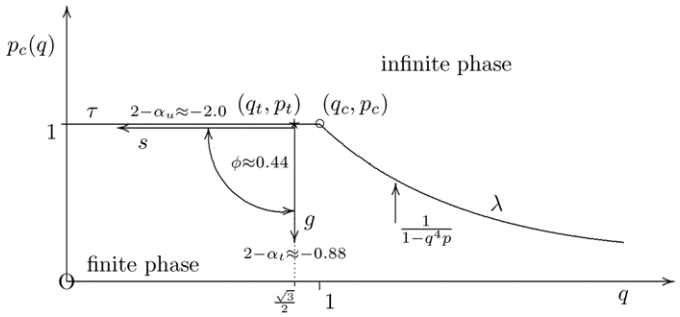

Figure 6. A schematic plot of $p_c(q)$. This is also the phase diagram of plane partition polygons in a volume–area ensemble, with the phase boundary $p_c(q)$ separating a finite and an infinite phase. $p_c(q)$ is a line of essential singularities in the generating function from $(0, 1)$ to the tricritical point $(q_c, p_c) = (1, 1)$, and it continues as a curve of poles in the generating function along the curve $q^4p = 1$. Along $p_c(q)$ the generating function is finite for $q \in [0, q_t)$, but it diverges for $q \in [q_t, 1)$. Multicritical scaling is found around the point $(q_t, p_t) \approx (0.866, 1)$. We set up scaling axes at the multicritical point (q_t, p_t) with the g-axis transverse to the critical curve and pointing down, while the s-axis is along the line $p = 1$, but pointing towards the left. The generating function $P_p(p, q)$ diverges along the g- and s-axes on approaching the multicritical point. Standard scaling assumptions show that $P_p(p, q) \sim g^{2-\alpha_t}$ along the g-axis as $g \to 0^+$, while $P_p(p, q) \sim s^{2-\alpha_u}$ along the s-axis as $s \to 0^+$ and our simulations show that $2-\alpha_t \approx -0.88$ and $2-\alpha_u \approx -2.0$. The crossover exponent can be determined from these results: we found that $\phi \approx 0.44$.

Arguments similar to the above show that the curves $pq^{4m} = 1$ are singular curves in the pq-plane. For $q \leqslant 1$ these accumulate on $p = 1$, so that the line $p = 1$ is a locus of essential singularities in $P_p(p, q)$. We shall provide numerical evidence below that $P_p(1, q) < \infty$ if $0 \leqslant q < q_t$, and the value of q_t will be estimated by statistical analysis of our data.

The phase diagram is plotted in figure 6. The critical curve $p_c(q)$ is separated into two parts by the critical point at (q_c, p_c). The first part is the line segment along $p = 1$ and this is a line of first order phase transitions (marked by τ in figure 6) which ends in a tricritical point at $(q_c, p_c) = (1, 1)$. The critical curve continues from this point in a curve of simple poles which is a λ-line of continuous transitions. The phase diagram is illustrated in figure 6, which should be compared to figure 10 in [24].

4.1.1. The area of plane partition vesicles along $p = 1$. The behaviour of the generating function $P_p(p, q)$ close to the point at $(q, p) = (q_t, 1)$ should be analysed to determine the scaling properties of plane partitions. Define the scaling field $s = (q_t - q)$ (so that $s \approx -\log(q/q_t)$ as q approaches q_t), then equation (30) suggests that

$$P_p(1, q) \sim \frac{\mathrm{e}^{\alpha s}}{s^{\gamma_s}} \qquad \text{as} \quad q \nearrow q_t, \tag{45}$$

where α is a constant, and γ_s an exponent to be determined. The mean area of plane partition vesicles along the line $p = t = 1$ and $0 \leqslant q < q_t$ is given by the derivative of $\log P_p(1, q)$ to $\log q$. Assuming that there is a constant C so that $P_p(1, q) = C\,\mathrm{e}^{\alpha s}/s^{\gamma_s}$ then suggests that

$$\langle \text{Area} \rangle \approx q_t \left(\frac{\gamma_s}{s} - \alpha \right). \tag{46}$$

In other words, the area should diverge proportional to γ_s/s as the critical point is approached.

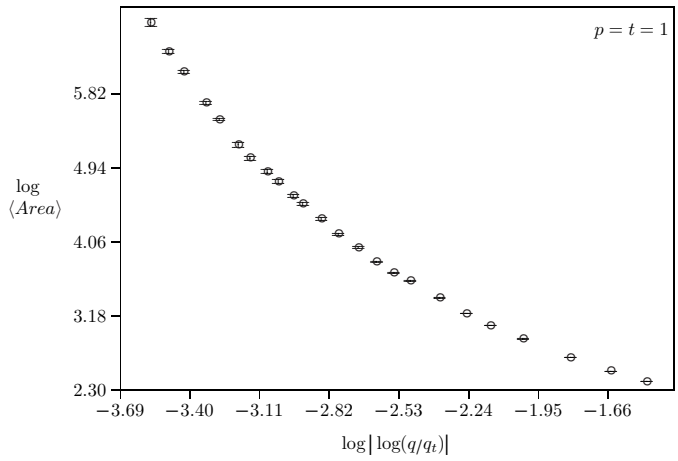

Figure 7. The logarithm of the mean area of plane partition vesicles for $p = t = 1$ as a function of $\log|\log(q/q_t)|$. The critical value of q is $q_t \approx 0.846\,70$, and this was determined by a least squares analysis of these data points assuming the model in equation (47).

In figure 7 the results of a simulation with $p = t = 1$ and $q \leqslant q_t$ using algorithm plane partition are displayed. By examining equation (46), and by noting that $-\log(q/q_t) \approx (1 - q/q_t)$, the mean area data should be described by the model

$$\log\langle\text{Area}\rangle = A - \log(-\log(Bq)) + C\log q + D\log^2 q. \tag{47}$$

While there are obvious short-comings in this model (the coefficient of the term $\log(-\log(Bq))$ is fixed at 1); the main purpose here is the determination of B, and this will fix the value of q_t. Since the term $\log(-\log(Bq))$ is the only divergent term on the right-hand side, and since the divergence in $\log\langle\text{Area}\rangle$ is expected to be proportional to $\log(-\log(Bq))$, one may assume that a successful least squares analysis with this model should approximate the location of the multicritical point $q_t = 1/B$.

Least square fits of the data to the model in equation (47) were performed to estimate B. The least squares error χ^2_N on N degrees of freedom was tracked to determine goodness-of-fit while data were discarded at values of q less than some minimum cutoff $q_{\min}$. χ^2_N is distributed as a χ^2-statistic on N degrees of freedom, and a fit was deemed statistically acceptable if χ^2_N is acceptable at the 95% level.

Acceptable fits were found for $q_{\min} \geqslant 0.7967$. For $q_{\min} = 0.7967$ the least square error was $\chi^2_{13} \approx 13.0$ on 13 degrees of freedom, acceptable at the 55.2% level. In this case, the estimate for B is $B = 1.181\,05 \pm 0.000\,38$. Discarding another data point by increasing $q_{\min}$ to 0.8011 produced $B = 1.181\,24 \pm 0.000\,40$ with $\chi^2_{12} = 12.3$ on 12 degrees of freedom, acceptable at the 57.7% level. Thus, our best estimate for B is

$$B = 1.181\,05 \pm 0.000\,38. \tag{48}$$

Since $B = 1/q_t$, this estimate gives

$$q_t = 0.846\,70 \pm 0.000\,28 \tag{49}$$

for the critical point q_t. The location of this critical point is close to $\sqrt{3}/2 = 0.866\,025\ldots$, but the error bar (which is one standard deviation) excludes this value. However, we are not able to account for sources of possible systematic errors due to inadequacies in our model, and so we cannot rule out the possibility that $q_t = \sqrt{3}/2$.

The results above do not verify the assumption in equation (45). By assuming that $1/q_t = 1.181\,05 \pm 0.000\,38$ determines the location of the critical point, and by approximating $-\log(1.181\,05q) \approx (1 - 1.181\,05q)$, a suitable alternative model for the mean area of plane partition vesicles is

$$\frac{\log\langle\text{Area}\rangle}{\log(1-1.181\,05q)} = \frac{\alpha}{\log(1-1.181\,05q)} - \rho + C\log(1.181\,05q) + D\log^2(1.181\,05q), \tag{50}$$

which includes terms to account for deviations from linearity in figure 7 for small values of q.

The value of ρ should be determined by a linear regression. Acceptable least squares fits were obtained for $q_{\min} = 0.7145$ ($\chi^2_{18} \approx 23.9$, acceptable at the 84.7% level), where $\rho = 1.3449 \pm 0.0020$. For $q_{\min} = 0.7361$, the regression shows that $\rho = 1.3438 \pm 0.0024$, and for $q_{\min} = 0.7578$, $\rho = 1.3396 \pm 0.0030$. In other words, these results are consistent and our best estimate for ρ is

$$\rho = 1.3449 \pm 0.0020. \tag{51}$$

Since $\rho \approx 4/3$, the mean area diverges as $q \nearrow q_t$ by

$$\langle\text{Area}\rangle \sim [-\log(q/q_t)]^{-\rho} \tag{52}$$

where $q_t = 0.846\,70 \pm 0.000\,28 \approx \sqrt{3}/2$ and where one may conjecture that $\rho = 4/3$. This result has implications for the assumption in equation (45). A divergence of the area proportional to $s^{-4/3}$ can be obtained if we assume that

$$P_p(1,q) \sim \frac{\mathrm{e}^{\alpha/s^{1/3}}}{s^{\gamma_s}} \tag{53}$$

instead. This assumption modifies the divergence of the mean area to

$$\langle\text{Area}\rangle \approx q_t\left(\frac{\alpha}{3s^{4/3}} + \frac{\gamma_s}{s}\right), \tag{54}$$

where $s = (q_t - q) \approx \log(q_t/q)$ when $q \nearrow q_t$.

To determine the exponent γ_s in equation (45) is numerically much more difficult. Its contribution to the mean area is secondary to the primary contribution made by the exponential term. By equation (54), one may examine the model

$$s^{4/3}\langle\text{Area}\rangle = A + q_t s^{1/3}\gamma_s + Cs + Ds^2. \tag{55}$$

Linear least squares analyses gave estimates for γ_s, and the quality of the estimates deteriorated quickly with increasing $q_{\min}$. A regression with $q_{\min} = 0.1732$ has $\chi^2_{26} = 31.9$ acceptable at the 80.3% level. This gives $q_t\gamma_s = 1.633 \pm 0.033$. Increasing $q_{\min} = 0.2598$ gives $q_t\gamma_s = 1.772 \pm 0.048$, and this estimate excludes the first by more than two standard deviations. Further increases in $q_{\min}$ gives the estimates 1.631 ± 0.065, 1.735 ± 0.086, 2.08 ± 0.13, 2.55 ± 0.21, 2.48 ± 0.37 and 2.73 ± 0.48. The last estimate contains all but smallest few of the previous within its 95% confidence interval. In fact, increasing $q_{\min}$ again gives the smaller estimates 2.11 ± 0.65 and 1.14 ± 0.98. All these results are statistically acceptable. If a weighted average is taken over all these results, then $q_t\gamma_s \approx 1.7$, with an unknown statistical and systematic error. In other words, the spread of results for γ_s has such large statistical uncertainties that they do not differ statistically from the results of the regressions at small $q_{\min}$. Thus we take as our best estimate $q_t\gamma_s \approx 1.7$, and if we assume that $q_t = \sqrt{3}/2$, then

$$\gamma_s \approx 2.0. \tag{56}$$

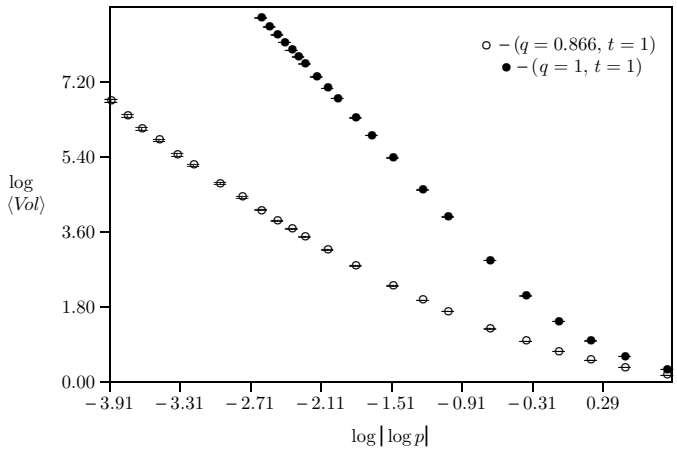

Figure 8. The logarithm of the mean volume of plane partitions as a function of $\log|\log p|$. The data denoted by ○'s were obtained by putting $q = q_t \approx 0.866$ and $t = 1$, while the data denoted by •'s were obtained when $q = t = 1$.

4.1.2. The volume of plane partition vesicles along $q = q_t$. Next, we put $q = q_t$ and consider the volume of plane partition vesicles as $p \nearrow 1$. While our best estimate for q_t in equation (49) is slightly smaller than $\sqrt{3}/2 \approx 0.866$, we approximated q_t by 0.866 and collected data. Our results are plotted in figure 8.

As before, we define $P_p(p, q_t) \equiv P_p(p, q_t, 1)$. In analogy with equation (30) one may assume that

$$P_p(p, q_t) \sim \frac{e^{\alpha g}}{g^{\gamma_g}}, \tag{57}$$

where $g = -\log p$ is the scaling field, and where α is a constant and γ_g is an exponent. This assumption suggests that the mean volume of plane partition vesicles along the line $q = q_t$ diverges as $\langle\text{Volume}\rangle \sim \gamma_g/g - \alpha$. However, this model did not describe the data in figure 8 well. We could not perform least squares regressions that were statistically acceptable. Instead, exploratory calculations suggested that $\langle\text{Volume}\rangle \sim 1/g^2$. This would be consistent with the ansatz that

$$P_p(p, q_t) \sim \frac{e^{\alpha/g}}{g^{\gamma_g}}, \tag{58}$$

and if we assume that $P_p(p, q_t) = Ce^{\alpha/g}/g^{\gamma_g}$, then this predicts that

$$\langle\text{Volume}\rangle \approx \frac{\alpha}{g^2} + \frac{\gamma_g}{g}. \tag{59}$$

Thus, a suitable model for the divergence in the mean volume of plane partition vesicles along the line $q = q_t$ and $t = 1$ is

$$\log\langle\text{Volume}\rangle = A + B\log(-\log p) + C\log p + D\log^2 p, \tag{60}$$

where B should be equal to -2. Our data fit this model well, and acceptable regressions were obtained by discarding data at values of p less than $p_{\min} = 0.5$. In this regression, $B = -1.971 \pm 0.012$ with least squares error $\chi^2_{12} = 19.2$ acceptable at the 91.5% level. If $p_{\min} = 0.6$, then $B = -2.018 \pm 0.017$ with $\chi^2_{11} = 11.3$, acceptable at the 57.5% level. These results are consistent with the assumption in equation (58).

Next, we attempt to determine the exponent γ_g in equations (58) and (59). Equation (59) suggests that

$$g^2\langle\text{Volume}\rangle = \alpha + \gamma_g g + Cg^2 + Dg^3 \tag{61}$$

as a suitable model for the data. The data fit this model well, and acceptable regressions were found by discarding data points at small values of p less than $p_{\min} = 0.2$. This gives $\gamma_g = 0.945 \pm 0.012$ with weighted least squares error $\chi^2_{16} = 24.5$ acceptable at the 91.9% level. Increasing $p_{\min} = 0.3$ gives $\gamma_g = 0.904 \pm 0.016$, and for $p_{\min} = 0.4$ one obtains $\gamma_g = 0.867 \pm 0.023$. The last estimate includes the previous in its 95% confidence interval, but excludes the first estimate. Hence, there appears to be a systematic drift in the estimate as $p_{\min}$ is increased, and we assume the estimate at $p_{\min} = 0.3$ (where $\gamma_g = 0.904 \pm 0.016$) as our first reliable estimate. Increasing $p_{\min}$ further to 0.5, 0.6 and 0.7 gave $\gamma_p = 0.851 \pm 0.035$, $\gamma_p = 0.754 \pm 0.058$ and $\gamma_p = 0.689 \pm 0.093$, respectively. In each case the estimate includes the previous in its 95% confidence interval, but there appears to be still a downwards trend, offset in some respect by a quickly rising confidence interval. By taking the weighted average of these results for $0.3 \leqslant p_{\min} \leqslant 0.7$, our best estimate for γ_g is

$$\gamma_g \approx 0.88. \tag{62}$$

4.1.3. The volume of plane partition vesicles along $q = 1$. Next we consider the mean volume of plane partition vesicles along the line $q = t = 1$. Data on the mean volume of plane partition vesicles were collected in this ensemble and are plotted in figure 8. The model

$$\log\langle\text{Volume}\rangle = A + B\log(-\log p) + C\log p + D\log^2 p \tag{63}$$

is again successful at modelling the data. A weighted least squares regression is acceptable at the 33.4% level if data corresponding to $p < p_{\min} = 0.4$ are discarded $\left(\chi^2_{14} = 11.3\right)$, in which case $B = -2.881 \pm 0.010$. Increasing $p_{\min} = 0.5$ shows that $B = -2.909 \pm 0.015$, acceptable at the 17.1% level and consistent with the result at $p_{\min} = 0.4$. This result is consistent with the ansatz that

$$P_p(p, 1) \sim \frac{\mathrm{e}^{\alpha/g^\kappa}}{g^{\gamma'_g}}, \tag{64}$$

where $g = -\log p$ is the scaling field, and where the exponent κ should have value close to 1.9 (since the regression above shows that $B \approx -2.881$). In particular, it seems plausible that $\kappa = 2$.

It is possible to test this prediction directly by approximating $P_p(p, 1)$ using the Euler–Maclaurin formula. Direct computation shows that

$$\log P_p(p, 1) = \frac{\mathcal{L}i_2(p)}{|\log p|} + \frac{\text{Polylog}(3, p)}{|\log p|^2} - \frac{\log(1-p)}{2} + R_1 \tag{65}$$

where $\text{Polylog}(m, p) = \sum_{j=1}^{\infty} p^j/j^m$ is the polylog-function and where the remainder term R_1 is bounded by

$$|R_1| \leqslant |\log(1-p)| + \left|\frac{p\log p}{1-p}\right| \simeq |\log(1-p)| \qquad \text{as} \quad p \nearrow 1. \tag{66}$$

This approximation is not uniform, but is still very accurate. For $p = 0.9$ we obtain $P_p(0.9, 1) = 107.93\ldots$ while the approximation gives $108.04\ldots$ and the bound on R_1 is $0.27\ldots$. For $p = 0.99$ we get $P_p(0.99, 1) = 11\,899.91\ldots$, the approximation is $11\,900.21\ldots$ and the remainder term is bound by $0.46\ldots$.

Since both $\mathcal{L}i_2(p)$ and Polylog$(3, p)$ are finite at $p = 1$, we get that $P_p(p, 1)$ is given by

$$P_p(p, 1) \approx \frac{\exp(\alpha_0/g + \alpha_1/g^2)}{\sqrt{g}\, f(g)} \tag{67}$$

where we approximate $g = -\log p \approx 1 - p$, and where by examining R_1, $f(g) \sim g$. This result would replace κ in equation (64) by 2 (as we expected), and assign the value $\gamma'_g = 3/2$ to the exponent.

4.1.4. Discussion. The assumptions in equations (45), (58) and (64) have certain consequences for the scaling of the area and volume of plane partition vesicles. In particular, along the line $p = t = 1$ and $q < q_t$, one expects the mean area to diverge as in equation (46), and the mean volume to diverge along the line $q = q_t, t = 1$, and $p < 1$ as in equation (59). Scaling assumptions in equation (21) can be compared with equations (45) and (58). In this case we note that the scaling uncovered by the numerical simulations are reminiscent of the scaling observed in partition polygons in equations (19) and (20). In particular, the critical value of q if $p = 1$ is $q_t = 0.846\,70 \pm 0.000\,38$ while the critical curve is given by $p = 1$ if $q \leqslant 1$ and $p = 1/q^4$ if $p > 1$. This is illustrated in figure 6.

Multicritical scaling is exhibited in the vicinity of the point $(q_t, p_t) \approx (\sqrt{3}/2, 1)$, and the multicritical scaling exponents of this scaling is approximated by

$$P(1, q, 1) \sim \frac{\mathrm{e}^{\alpha/s^{1/3}}}{s^{2.0}}, \qquad \text{where} \quad s = -\log(q/q_t); \tag{68}$$

$$P(p, q_t, 1) \sim \frac{\mathrm{e}^{\beta/g}}{g^{0.88}}, \qquad \text{where} \quad g = -\log p. \tag{69}$$

Thus, one may identify the exponents

$$2 - \alpha_u \approx -2.0, \qquad 2 - \alpha_t \approx -0.88, \tag{70}$$

and approximate the crossover exponent

$$\phi = \frac{2 - \alpha_t}{2 - \alpha_u} \approx 0.44. \tag{71}$$

This is sufficiently close to $1/2$ that one may make the qualified conjecture that $\phi = 1/2$ in this model.

5. Conclusions

In this paper we first reviewed the multicritical scaling of partition polygons, and used those results to examine the presumed multicritical scaling of plane partition vesicles by numerical means. Our main result is that the generating function $P_p(p, q)$ exhibits multicritical scaling close to the point $(q, p) = (\sqrt{3}/2, 1)$. This point does not coincide with the critical point at $(q_c, p_c) = (1, 1)$ where there is a thermodynamic phase change in the model, and which is also a tricritical point in the phase diagram. At this point the vesicles undergo an inflation–deflation transition, and the nature of the singularities in the generating function along the critical curve changes from essential singularities into simple poles. The multicritical scaling regime however is displaced to a different location near the point $(q_t, p_t) = (\sqrt{3}/2, 1)$ not coincident with the tricritical point.

In equations (45) and (58) scaling assumptions for the generating function close to the multicritical point is made which are consistent with our numerical data. These assumptions allow the estimation of the crossover exponent ϕ, which apparently should be close to $1/2$.

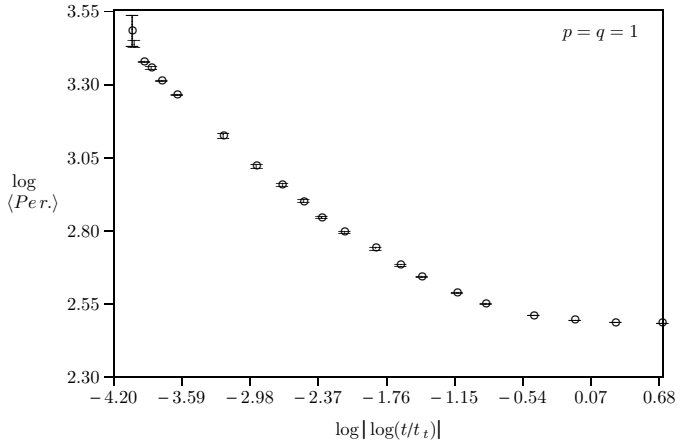

Figure 9. The logarithm of the mean perimeter of plane partition vesicles as a function of $\log|\log(t/t_t)|$ for $p = q = 1$ and where $t_t \approx 0.7541$.

Plane partition vesicles should also be considered in the qt- and pt-planes. These require the simulation of plane partition vesicles as a function of t with $p = q = 1$ to determine the multicritical value t_t of t. Analogous to equation (45), one may propose that

$$P_p(1, 1, t) \sim \frac{e^{\alpha g_t}}{g_t^{\gamma_t}} \qquad \text{as} \quad t \nearrow t_t, \tag{72}$$

where γ_t is a critical exponent to be determined. The scaling field g_t should be proportional to $t_t - t$ or to $-\log(t/t_t)$, and α is a constant. Taking the derivative to g_t of $\log P_p(p, q, t)$ shows that the mean perimeter of plane partitions increases as

$$\langle\text{Perimeter}\rangle = t_t \left(\frac{\gamma_t}{g_t} - \alpha \right). \tag{73}$$

In other words, the perimeter should diverge inversely proportional to g_t as the critical value of t is approached when $p = q = 1$.

We collected data on the mean perimeter of plane partition vesicles over several runs with $p = q = 1$. Numerical convergence was very slow, and only with a tremendous amount of computer time did we succeed in collecting the data in figure 9. There is a sharp transition when t is close to t_t, and our data suggest that $t_t \approx 0.75$. For $t > 0.74$, each data point corresponds to a Monte Carlo simulation with 5×10^{10} attempted elementary moves. Autocorrelation times quickly increased in this regime, and the quality of the measurements deteriorated with increasing t. The largest value of t plotted in figure 9 is $t = 0.7465$, still well short of 0.75.

Nonlinear least squares analysis of the data, assuming the model

$$\log\langle\text{Perimeter}\rangle = A - \log(-\log(Bt)) \tag{74}$$

were generally not successful. We adapted this to the assumption

$$\log\langle\text{Perimeter}\rangle = A - C\log(-\log(Bt)) \tag{75}$$

and performed least squares analysis. The least square error was tracked as a function of the minimum value of t in the data. We discarded data at small values of t until a fit acceptable at the 95% level was obtained. The fits were unacceptable until $t_{\min} = 0.675$, where $\chi^2 \approx 10.2$ on 9 degrees of freedom, acceptable at the 66.6% level. In this case the parameters were

$B = 1.3260 \pm 0.0012$ and $C = 0.2658 \pm 0.0076$ (95% confidence intervals). We observed that by increasing $t_{\min}$ yet again, that these estimates remained inside their confidence intervals, and we accepted these as our best estimates.

Our best estimate for t_t is $t_t = 1/B = 0.754\,14 \pm 0.000\,64$. A heuristic argument similar to that for partition polygons (see figure 4) suggests that $t_t = 3^{-1/4} = 0.7598\ldots$. This value is outside the confidence interval of our estimate, but we did not consider the effects of systematic errors in our data. The power-law dependence in equation (75) is similar to the assumption in equation (52) for the mean area of plane partition vesicles. However, our data were not secure enough for a confident conjecture on the power-law dependence of the mean perimeter.

By approximating $-\log(t/t_t) \approx (1 - t/t_t)$, a suitable model of the mean perimeter of plane partition vesicles would be

$$\frac{\log\langle\text{Perimeter}\rangle}{\log(1 - t/t_t)} = \frac{\alpha}{\log(1 - t/t_t)} - \beta + C(1 - t/t_t) + D(1 - t/t_t)^2. \tag{76}$$

The value of β can be determined by a linear least squares analysis of the data. Acceptable regressions were obtained with $t_{\min} = 0.20$ ($\chi^2_{16} \approx 11.82$, acceptable at the 25% level) where $\beta = 0.1891 \pm 0.0010$. Increasing $t_{\min}$ to 0.30 gives $\beta = 0.1899 \pm 0.0019$ acceptable at the 30% level on 15 degrees of freedom. Thus, β is close to 1/5, and it appears that the mean perimeter diverges as $\langle\text{Perimeter}\rangle \sim [-\log(t/t_t)]^{-1/5}$. However, the data on the mean perimeter of plane partition vesicles were not convincing, and this estimate should be considered as a preliminary result.

Acknowledgment

EJJvR is supported by an operating grant from NSERC (Canada).

References

[1] Banavar J R, Maritan A and Stella A L 1991 Geometry, topology, and universality of random surfaces *Science* **252** 825–7
[2] Banavar J R, Maritan A and Stella A L 1991 Critical behaviour of two-dimensional vesicles in the deflated regime *Phys. Rev.* A **43** 5752–4
[3] Bousquet-Mélou M 1992 Convex polyominoes and heaps of segments *J. Phys. A: Math. Gen.* **25** 1925–34
[4] Bousquet-Mélou M and Viennot X G 1992 Empilements de segments et q-énumération de polyominos convexes ddirigés *J. Comb. Theory* A **60** 196–224
[5] Brak R and Owczarek A L 1995 On the analyticity properties of scaling functions in models of polymer collapse *J. Phys. A: Math. Gen.* **28** 4709–25
[6] Brak R, Owczarek A L and Prellberg T 1993 A scaling theory of the collapse transition in geometric cluster models of polymers and vesicles *J. Phys. A: Math. Gen.* **26** 4565–79
[7] Brak R, Owczarek A L and Prellberg T 1994 Exact scaling behaviour of partially convex vesicles *J. Stat. Phys.* **76** 1101–28
[8] Bressoud D M 1999 The story of the alternating sign matrix conjecture *Proofs and Confirmations* (Cambridge: Cambridge University Press)
[9] Buzano C and Pretti M 2002 Lattice polymers with hydrogen bond-like interactions *J. Chem. Phys.* **117** 10360–9
[10] Foster D P and Seno F 2001 Two dimensional self-avoiding walk with hydrogen-like bonding: phase diagram and critical behaviour *J. Phys. A: Math. Gen.* **35** 9939–57
[11] Hardy G H and Ramanujan S 1918 Asymptotic formulae in combinatorial analysis *Proc. London Math. Soc. Ser. 2* **17** 75–115
[12] Janse van Rensburg E J 1990 The topology of interfaces *J. Phys. A: Math. Gen.* **23** 5879–95
[13] Janse van Rensburg E J 1992 Surfaces in the hypercubic lattice *J. Phys. A: Math. Gen.* **25** 3529–47
[14] Janse van Rensburg E J 1994 Statistical mechanics and topology of surfaces $\mathcal{Z}d$ *J. Knot Theory Ram.* **3** 365–78
[15] Janse van Rensburg E J 1997 Crumpling self-avoiding surfaces *J. Stat. Phys.* **88** 177–200
[16] Janse van Rensburg E J 2000 *The Statistical Mechanics of Interacting Walks, Polygons, Animals and Vesicles* (New York: Oxford University Press)

[17] Janse van Rensburg E J 2000 Interacting columns: generating functions and scaling exponents *J. Phys. A: Math. Gen.* **33** 7541–54
[18] Janse van Rensburg E J 2004 Inflating square and rectangular lattice vesicles *J. Phys. A: Math. Gen.* **37** 3903–32
[19] Klarner D 1965 Some results concerning polyominoes *Fibonacci Q.* **3** 9–20
[20] Klarner D 1967 Cell growth problems *Can. J. Math.* **19** 851–63
[21] Klarner D and Rivest R 1973 A procedure for improving the upper bound for the number of n-Ominoes *Can. J. Math.* **25** 585–602
[22] Klarner D and Rivest R 1974 Asymptotic bounds for the number of convex n-Ominoes *Discrete Math.* **8** 31–40
[23] Kuperberg G 1996 Another proof of the alternating sign matric conjecture *Int. Math. Res. Notes* **1996** 139–50
[24] Lawrie I D and Sarbach S 1984 Theory of tricritical points *Phase Transitions and Critical Phenomena* vol 9 ed C Domb and J L Lebowitz (London: Academic Press) pp 65–191
[25] MacMahon P A 1912 Memoir on the theory of partitions of numbers—part V. Partitions in two-dimensional space, to which is added an adumbration of the theory of partitions in three-dimensional space *Phil. Trans. R. Soc.* **211** 75–110 (See: *Percy Alexander MacMahon: Collected Papers*, ed G E Andrews, vol 1, pp 1328–63)
[26] MacMahon P A 1899 Partitions of numbers whose graphs possess symmetry *Trans. Camb. Phil. Soc.* **17** 149–70
[27] MacMahon P A 1912 Memoir on the theory of partitions of numbers—part VI. Partitions in two-dimensional space *Phil. Trans. R. Soc.* **211** 345–73 (See: *Percy Alexander MacMahon: Collected Papers*, ed G E Andrews, vol 1, pp 1404–34)
[28] Madras N N and Sokal A D 1988 The pivot algorithm: a highly efficient Monte Carlo method for the self-avoiding walk *J. Stat. Phys.* **47** 573–95
[29] Orlandini E and Tesi M C 1992 Monte carlo study of three dimensional vesicles *Physica* A **185** 160–5
[30] Orlandini E, Stella A L, Einstein T L, Tesi M C, Beichl I and Sullivan F 1996 Bending rigidity driven transition and crumpling point scaling of lattice vesicles *Phys. Rev.* E **53** 5800–7
[31] Pólya G 1969 On the number of certain lattice polygons *J. Comb. Theory* **6** 102–5
[32] Prellberg T and Owczarek A L 1995 Stacking models of vesicles and compact clusters *J. Stat. Phys.* **78** 701–30
[33] Read R C 1962 Contributions to the cell growth problem *Can. J. Math.* **14** 1–20
[34] Richard C 2002 Scaling behaviour of two-dimensional polygon models *J. Stat. Phys.* **108** 459–93
[35] Serra P, Stilck J F, Cavalcanti W L and Machado K D 2004 Polymers with attractive interactions on the Hussimi lattice *J. Phys. A: Math. Gen.* **37** 8811–21
[36] Wright M E 1931 Asymptotic partition formulae I. Plane partitions *Q. J. Math. Oxford Ser.* **II** 177–89
[37] Wright M E 1968 Stacks *Q. J. Math.* **19** 313–20
[38] Zeilberger D 1996 Proof of the alternating sign matrix conjecture *Electron. J. Comb.* **3** R3
[39] Zeilberger D 1996 Proof of the refined alternating sign matrix conjecture *New York J. Math.* **2** 59–68